LA-UR-12-00139

Approved for public release; distribution is unlimited.

Title:	MESH HUMAN PHANTOMS WITH MCNP (U)
Author(s):	Casey A. Anderson Karen C. Kelley John T. Goorley
Intended for:	Simulia Customer Conference, Providence, RI May 15 - 17, 2012

Form 836 (7/06)

MESH HUMAN PHANTOMS WITH MCNP

Casey A. Anderson
W-13: Advanced Engineering Analysis, Los Alamos National Laboratory, Los Alamos, New Mexico, 87545

Karen C. Kelley
W-13: Advanced Engineering Analysis, Los Alamos National Laboratory, Los Alamos, New Mexico, 87545

John T. Goorley
XCP-3: Computational Physics, Los Alamos National Laboratory, Los Alamos, New Mexico, 87545

Abstract

Improvements in technology and computing have provided highly detailed representations of the human body for biomedical simulations. One specific application of these models is using the geometry to develop human phantoms for particle transport applications in MCNP, a general purpose particle transport code developed by Los Alamos National Laboratory. Traditional mathematical based phantoms, such as the ICRP 23 "Reference Man" MIRD-5 adult male and the Snyder Phantom, use equations to specify the surfaces and volumes of organs within the body, while image based models, such as the *Visible Photographic Man* (VIP-Man) and *Virtual Family* models, use segmented CT and MRI data to construct a three dimensional model of the body in solid, voxelized, or unstructured mesh form. Image based models required voxelization to run in MCNP, producing a tradeoff between anatomical accuracy and computational expense based on voxel size, while mathematical based models only provided a crude representation of the human anatomy. The most recent release of MCNP allows unstructured meshes, generated from Abaqus CAE®, to be imported as an alternative geometry to the the traditional constructive solid geometry (CSG), increasing the geometric accuracy and potentially improving computational run time compared to voxelized models. This new capability also provides improved visualization capabilities, the ability to isolate by parts (for visualization and source specification), flux and dose information for each element, multiphysics FEA of the mesh, and the potential for patient specific models with reconstruction software already in use (such as 3D-Doctor®). This report demonstrates these new capabilities of MCNP, specifically the use of unstructured mesh human phantoms for health physics and medical applications.

January 13, 2012

I. Introduction

Computational human phantoms used for dose calculations require an appropriate geometry representation and realistic radiation interaction data[12] conforing to the ICRP 23 Reference Man.[10,11] Traditional *Mathematical Models* use mathememtical descriptions of planes and surfaces to create a representation of the human anatomy. Adjustments in these equations accomodate for population differences based on age, size, sex, and race. In the mid 1980s, image based *Tomographic Models* were developed, using segmented image data from CT and MRI scans to reconstruct a three-dimensional model of the body.[11] Another set of phantoms, not mentioned in the ICRU reports, are *Hybrid Models*, which use a combination of mathematical representations, specifically nonuniform rational B-spline (NURBS) surface modeling, and tomographic images to generate three-dimensional anatomical phantoms.[7]

Modeling the human anatomy with the ability to import for computational analysis often requires a trade-off between anatomical accuracy and computational expense. Mathematical models such as the MIRD-5 Adult Male and Snyder Head Phantom[11,14] are easily produced in MCNP legacy code, yet only provide a crude representation of the human anatomy. Tomographic models traditionally require voxelization to run in MCNP,[7] which can produce large, expensive and accurate models or smaller, less detailed models based on the voxelization seed size.[15] Eliminating the voxelization requirement would allow the legacy mesh (often NURBS or unstructured mesh) used as the standard geometry, as these models are generally developed using these methods. As stated by Lee et. al in 2008, "***The voxelization process is crucial for the resulting NURBS phantoms to be imported to radiation transport codes as currently there are no Monte Carlo codes available that can directly handle NURBS or polygon mesh geometry for radiation transport.***"[7]

The general purpose Monte Carlo transport code MCNP (Version 6),[6] developed at Los Alamos National Laboratory, has a new capability that allows particle transport on hybrid geometries. Unstructured mesh from Abaqus CAE® and legacy CSG geometries can be included in the same model. Complex geometries created in Abaqus CAE® no longer need to be simplified through processes such as voxelization or rewriting in MCNP legacy code, and now can be directly imported and retain their native CAE geometry. This paper discusses the use of these hybrid geometries in the form of unstructured mesh human phantoms for Monte Carlo dose calculations with MCNP, specifically comparison between several models currently in use.

II. Methods and Materials

The newest release of the general purpose Monte Carlo radiation transport code MCNP version 6, is used to demonstrate the new capability of using unstructured mesh phantoms in hybrid geometries for particle transport. Several voxelized computational phantoms were used in this testing: the Snyder head phantom,[14] the Zubal head model,[19] and the VIP-Man.[15] These models have been previously tested in MCNP[2,4] and are common phantoms used for computational medical physics applications.[5] Testing of the models with the hybrid geometries requires an unstructured mesh input deck, which voxelized models can be reconstructed into to meet this requirement. Alternative to the meshed voxelized models are Abaqus CAE® unstructured mesh models, where the primary focus is on implementing these models as reference phantoms instead of voxelized and mathematical models. The following sections describe the MCNP hybrid geometry capability, several phantoms used in testing, and the python script to convert voxelized phantoms into mesh inputs. Testing of more detailed and complete unstructured mesh phantoms is in progress.

A. MCNP6 Hybrid Geometry

The Monte Carlo development team (*XCP-3*) at Los Alamos National Laboratory has been developing the particle transport code MCNP for over 40 years, with most recent release being MCNP6. Abaqus CAE® is a Computer Aided Engineering (CAE) software developed by Simulia and Dassault Systèmes, used for designing mesh models that are used in finite element analysis. MCNP6 hybrid geometries embed the Abaqus-generated input file (.inp), which contains the mesh, part, assembly, and set data, within CSG geometries. A background and universe geometry in CSG is required for particle transport, and other geometries may also be included. Particle tracking occurs across the mesh and CSG universe, following a particle through the surfaces, tabulating interaction data that gets written to an "elemental edits" (.eeout) file.[6] The data in this file includes the particle flux and energy deposition, which can be converted into an ODB file and read into Abaqus for visualization and further multiphysics analysis.

B. Computational Phantoms

The development of computational phantoms for radiation dosimetry has been around since the 1960s,[11] increasing in complexity and detail with increasing computer resources. Full body models have been developed to accomodate for the size differences encounted by the general populations, factors include weight, BMI, race, sex, age, and pregnancy.[10,17] Mathematicial and hybrid based phantoms account for these differences by adjusting the equations and surfaces as needed,[7] while adjustments to tomographic models, though much more rigid, can also account for these differences.[17] Much

work has been done by Dr. X. George Xu et al. at RPI for his work on these computational phantoms for medical purposes, including the published book *Handbook of Anatomical Models for Radiation Dosimetry*.[17,18] Calculations of dose and interactions in the body requires accurate tissue data, found in the *ICRP Report 23 Reference Man*, and radiation interaction data, found in the *ICRU Report 46*.[10,12] Several of the computational phantoms used in this paper are described below. The MIRD mathematical computational phantom is shown below in Figure 1

B.i The *Visible Photographic Man*

The National Library of Medicine (NLM) has been developing anatomically detailed, three-dimensional representations of the male and female adult human bodies in the Visible Human Project® (VHP).[9] The VIP-Man is *an image based whole-body adult male model constructed from the color photographs of the Visible Human Project®*.[15] Voxelized modes of the VIP-Man, rangining in size from 0.33 mm x 0.33 mm x 1 mm resolution (3.7 billion voxels) to 4 mm x 4 mm x 4 mm resolution (5.9 million voxel models) were developed for use in MCNP, where the 4 mm model is commonly used as an optimized model for computational efficiency and accuracy.[2] A special thanks to Dr. George Xu at RPI for the complete and torso voxelized models of the VIP-Man which were head are used for testing in this report, shown below (*left*) in Figure 1. Surface based models of the VIP-Man, which produce unstructured mesh input decks, will hopefully soon be tested, a section shown in Figure 10.

B.ii Snyder & Zubal Head Phantom

The Snyder Head Phantom is a mathematical model developed in the 1960s that uses three ellipsoid equations defining the boundaries between the brain, skin, scalp, skin, and air, together representing the human skull.[4,11,14] Voxel models of the Snyder head were developed based on data from the analytical model, and both models were demonstrated in MCNP for reference dosimetry calculations.[4] The Zubal head phantom, named after one of the original developers Dr. George Zubal, is a tomographic model devloped in the 1990s at Yale University. Models were developed of the complete body, the torso, and more detailed model of the head,[19] with a voxelized mesh model shown below in Figure 2. A mathetmatical CSG section was added to the base of the voxelized Zubal head section complete the lower jaw and the neck. The hybrid Zubal model and the voxelized Snyder phantoms were used for testing.

B.iii Other Phantoms

There are many computational phantoms used today that represent the general population, most described in the ICRU Report 48, with newer versions described in the book *Handbook of Anatomical Models for Radiation Dosimetry, 1st edition*.[11,18] Some of these models include; the RPI-Adult Male (RPI-AM), RPI-Adult Female (RPI-AF), RPI-Pregnant Female (RPI-P), Female Adult mesh (FASH), Male Adult mesh (MASH), Virtual Family,[1] NORMAN phantom, the Korean, Japanese, and Chinese Computational Phantoms, and the MIRD phantoms.[11] The NURBS-based, Extended, and Mathematical cardiac-torso (NCAT, XCAT, MCAT, respectively) phantoms are based on the Visible Human from the NLM (similar to the VIP-Man), and provide imaging simulation (XCAT, MCAT) and 4D respiratory modeling (NCAT).[13] We are currently evaluating the NCAT and XCAT phantoms.

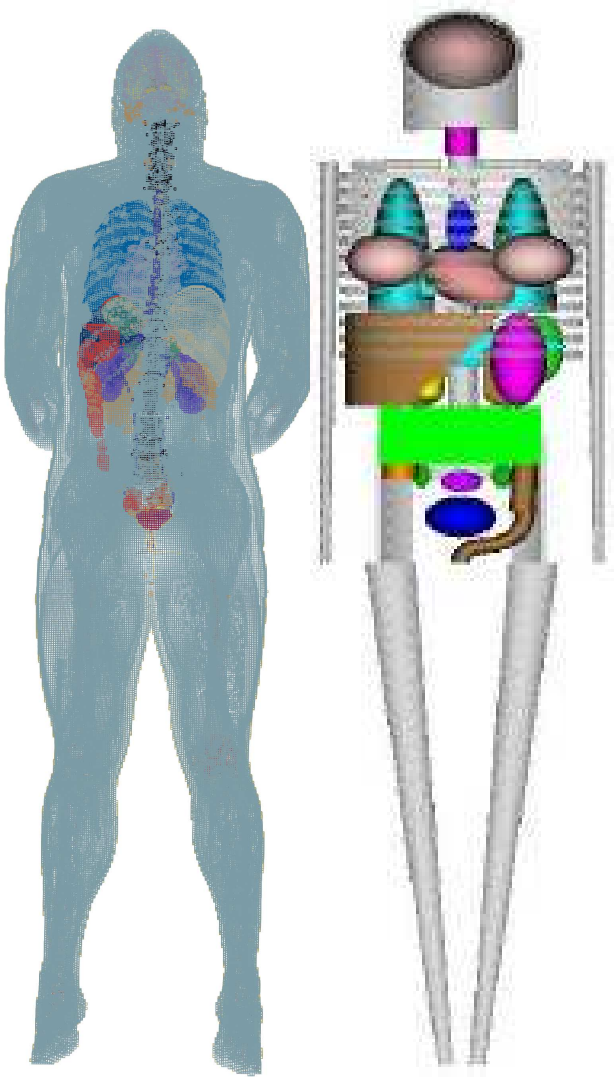

Figure 1: The image based 4 mm VIP-Man (*left*) and mathematical MIRD-5 Adult Male (*right*)

C. Voxel to Abaqus Script

Without surface-based or NURBS models of these image-based phantoms readily available, an alternate mesh generating process was needed for testing. A python script was developed that extracts data from the MCNP lattice geometry, generates an Abaqus/-

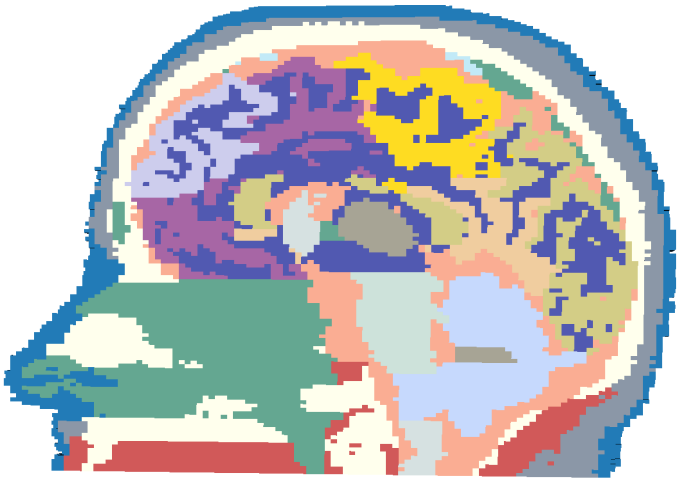

Figure 2: Saggital cut of the 61 part Zubal head phantom, viewed in Abaqus/CAE (*right*)

CAE mesh input file, and uses built-in methods in Abaqus/CAE to clean up the file (merge nodes, renumber elements). The generated files are easily read by Abaqus, separated into parts, and capable of running in MCNP6 with minor adjustments to the input deck. Default parts names are of the integer they represent (1=ONE,2=TWO..), but a separate reference file assigning an integer to a part name will name the parts accordingly. The MCNP lattice model and reconstructed Abaqus/CAE unstructured mesh model are the exact same geometry, and therefore are good benchmarks for testing and comparison. Comparison of the lattice geometry viewed with the native MCNP plotter and the mesh viewed in Abaqus/CAE are shown in Figure 3.

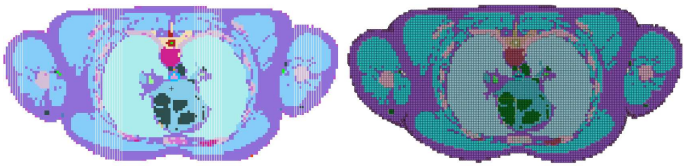

Figure 3: Transverse plane slice of the 4 mm VIP-Man in MCNP lattice geometry (*left*) and mesh based geometry in Abaqus/CAE (*right*)

III. Results

All computational results were completed on a Linux OS (RedHat) and a 2.67GHz Intel Xeon processor Model X5650

In this paper, we present the initial findings of using human phantom hybrid geometries for particle transport in MCNP6, currently limited to a few converted voxelized models and an unstructured chest and lung model. Converting the MCNP voxel data into an Abaqus/CAE mesh with the python script took several minutes for the 8 mm Snyder head model and up to 11 hours for the 4 mm VIP-Man, each using approximately 200 MB memory. Other models with 155 million elements took approximately 3 days and used 11 GB memory). The meshed model file sizes were larger than the CSG counterparts, with the Zubal head model 200 times larger, both VIP-Man models ˜40 times larger, and the Snyder models (both 4 mm and 8 mm) only three times larger. Since an MCNP lattice geometry requires a completely filled lattice, many voxels outside the main geometry are filled with air and can be removed from the mesh model with air as the background material. This reduces file sizes by nearly 50% and significant improvements in computational efficiency. The file sizes are compared in Table 2, and the mesh data is shown in Table 1.

Table 1: **Data of Voxelized Phantoms**[*]

	Parts	**Voxels**	**Nodes**
VIP-Man (Head to Torso)	41	321958	598848
VIP-Man (Whole Body)	61	1628350	2696172
Zubal Head	61	543338	894062
Snyder Head (8mm)	64	6488	28553
Snyder Head (4mm)	40	47448	159484
Pelvis	5	158878	239093
Lungs (Voxel)	1	54709	66139
Lungs (UM)**	1	24938	5797

[*] Data without the air voxels
[**] Unstructured Mesh Lungs Model

Table 2: **Geomtry File Size Comparison** (*MB)*

	CSG	**Mesh**	**Mesh**[+]
VIP-Man (Head to Torso)	4.3	178.6	53.0
VIP-Man (Whole Body)	19.3	830.2	270.1
Zubal Head	.72	150.9	82.6
Snyder Head (8mm)	.97	2.98	1.8
Snyder Head (4mm)	5.2	16.5	10.7
Pelvis	4.2	166.8	74.5
Lungs (Voxel)	—-	—-	7.4
Lungs (UM)	—-	—-	1.2

[+] Surrounding Air Voxels Removed from the Geometry

The hybrid geometries averaged longer run times for processing the geometry and particle tracking, shown in Tables 3 and 4, respectively. Threaded pre-processing

allowed parallel processing on separate parts, explaining the faster setup time of the larger 41-part VIP-Man compared to the slow setup of the 5-part male pelvis model. The CSG models of the Snyder Head phantoms were not represented by a repeated lattice and had a large number of parts for few elements, partially explaining the faster pre-processing time with the hybrid geometry. Removal of the outside air voxels sped up pre-processing significantly on the larger models (Zubal head and VIP-Man) with only slight improvements on the smaller Snyder models, but improved transport time significantly for the same model. Only the 8 mm Snyder Head phantom was used for transport with and without the surrounding air voxels to deomonstrate similar results. Other limitations with the hybrid geometries include a lack of variance reduction, which can increase computational efficiency, and no neutron kerma factors (for dose calculations with neutrons), though both will soon be implemented. For accurate comparison, all variance reduction and kerma factors were removed from the CSG models. Memory footprints of pre processing and transport are shown in Table 5 and Table 6, respectively.

Table 3: **MCNP6 Pre-Processing Time (*Min)***

	CSG	**Mesh**	**Mesh$^+$**
VIP-Man (Head to Torso)	1.02	998.2	25.2
VIP-Man (Whole Body)	4.82	—-	605.6
Zubal Head	0.97	411.1	18.7
Snyder Head (8mm)	0.19	0.34	0.16
Snyder Head (4mm)	0.50	0.61	0.48
Pelvis	0.25	423.3	50.52
Lungs (Voxel)	—-	—-	2.66
Lungs (UM)	—-	—-	0.28

$^+$ Surrounding Air Voxels Removed from the Geometry

Table 4: **100 million histories run time (*min)***

	CSG	**Mesh**	**Mesh$^+$**
VIP-Man (Head to Torso)	1551	—-	19006
VIP-Man (Whole Body)	1187	—-	36171
Zubal Head	2688		19715
Snyder Head (8mm)	1204	78509	17804
Snyder Head (4mm)	5490	—-	64580
Pelvis	930	—-	—-
Lungs (Voxel)	—-	—-	1173
Lungs (UM)	—-	—-	538.8

$^+$ Surrounding Air Voxels Removed from the Geometry

Table 5: **Pre-Processing Memory Footprint (MB)***

	CSG	**Mesh****
VIP-Man (Head to Torso)	100	1450
VIP-Man (Whole Body)	500	2014
Zubal Head	<100	1617
Snyder Head (8mm)	400	39
Snyder Head (4mm)	800	231
Pelvis	100	523
Lungs (Voxel)	—-	59
Lungs (UM)	—-	19

* CSG memory from *jtop*, accurate to .1 GB
** Air voxels removed, estimated value in output file

Table 6: **Transport Memory Footprint (MB)***

	CSG	**Mesh****
VIP-Man (Head to Torso)	100	800
VIP-Man (Whole Body)	1000	
Zubal Head	100	900
Snyder Head (8mm)	400	300
Snyder Head (4mm)	900	400
Pelvis	100	—-
Lungs (Voxel)	—-	100
Lungs (UM)	—-	100

* CSG, mesh memory from *jtop*, accurate to .1 GB
** Air voxels removed from the mesh

For initial results, the source that was specified in the original MCNP input deck was mainly used as the source in the hybrid model. The Snyder head models used a 10 cm photom beam as the source based on the models developed by Goorley et. al.[4] The Zubal head phantom and male pelvis used a similar photon source that simulates a radiotherapy treatment. The head and torso model of the VIP-Man used a posterior-anterior directional photon source, shown in Figure 7. Another run demonstrated the ability to specify a source location in the mesh by creating a source Set (*set_ source_ 001*) in Abaqus/CAE, such as an Iodine source in the thyroid, a common treatment for hyperthyroidism, shown in Figure 4. As the largest model, the complete VIP-Man model was irradiated using a whole body source to achieve converged results for each element within the model, shown in Figure 5.

The only true unstructured meshed models readily available were the chest and lung models of the RPI-

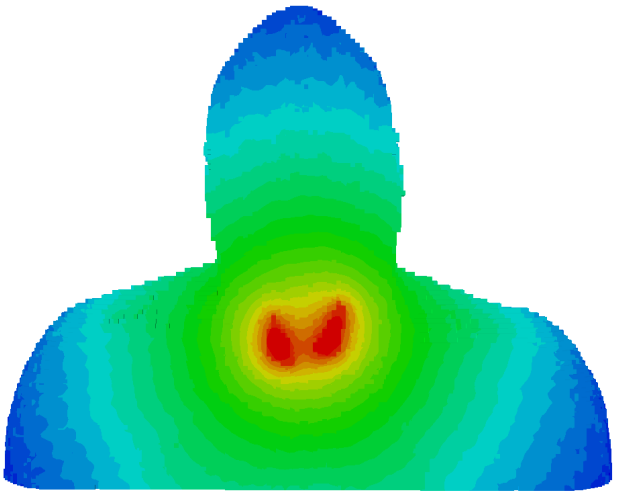

Figure 4: Simulating an Iodine source in the thyroid by creating a source Set in the thyroid of the 4 mm VIP-man

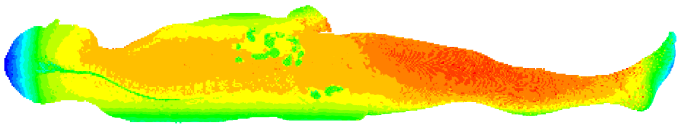

Figure 5: Whole body gamma irradiation source of the 4 mm VIP-Man

Adult Male. Extracting the lungs from the voxelized Abaqus model, these two models were used as a comparison of an unstructured model and voxelized model. For comparative purposes, an isotropic gamma source was placed between the lungs in both models. The unstructured lungs required half the elements and one-tenth the number of nodes as the voxelized model, resulting in a geometry file six times smaller, more intact geometry, and less than half the required transport time as the voxelized lung. Though the two models are different, this section demonstrates the significant improvement that true unstructured models have at improving geometrical accuracy at less computational expense. The resulting lung irradiation source is shown in Figure 9.

Mesh tallies overlay a regular mesh over the entire hybrid geometry and offer the ability to tally particle flux or energy deposition within the mesh. In this case, mesh tallies allows a direct comparison in flux between CSg and mesh geometries. The 8 mm Snyder head phantom was tested, comparing the mesh tallies to the CSG lattice tallies, and the tallies between the hybrid geometries with and without the air voxels. Though the same geometry, different random number walks resulted in large differences (10%) Figure 11. Removal of the air voxels also had similar results (.25% error) at 100 million histories, shown in Figure 12 and compared to one million

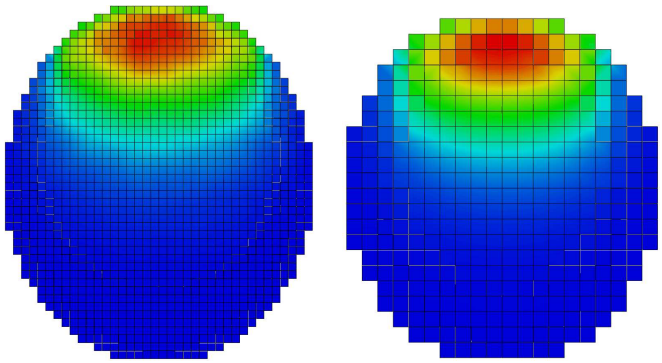

Figure 6: 10 cm monodirectional beam on the 4 mm (*left*) and 8 mm (*right*) voxelized Snyder Head phantom[4] viewed in Abaqus/CAE

histories in Figure 13. Dose error statistics were plotted for both the one million and 100 million runs in Figure 14.

IV. Discussion

This paper discusses the implementation of unstructured mesh human phantom geometries as use for radiological dose assessment. The reconstruction of these voxelized models into an Abaqus/CAE mesh creates nearly an exact replica of the geometry (error from numerical round-off in Abaqus), allowing for direct comparison of the hybrid geometries and the legacy MCNP lattice representation. Preliminary results from mesh tallies showed statistical agreement between the hybrid and CSG voxelized models from the Snyder Head phantom. Large models fared the worst computationally from the voxelized hybrid geometries to the CSG lattice, partially due to the large number of elements for each part. Adjustments in the voxel-to-abaqus script to divide large parts into separate parts could improve computational efficiency of the current models without altering the geometry, something that should be implemented and tested soon. Reconstructing voxelized models into an Abaqus mesh is not a computationally advantageous means for particle transport, as shown by the file size and computational results, since each element is described using nodes and connectivity instead of a single integer in the MCNP lattice. However, this process also described the added benefit of the hybrid geometries from improved visualization, source specification, and easy adjustments to the geometry such as the removal of the surrounding air voxels.

The use of a complete unstructured mesh human phantom, one which retains the anatomical accuracy from the tomographic model, is needed to complete this study. Outdated and voxelized models are being used only for proof-of-concept and comparative purposes, and are not demonstrating any significant breakthroughs with this new capability. The XCAT phantom will soon be received and tested, hopefully providing full function-

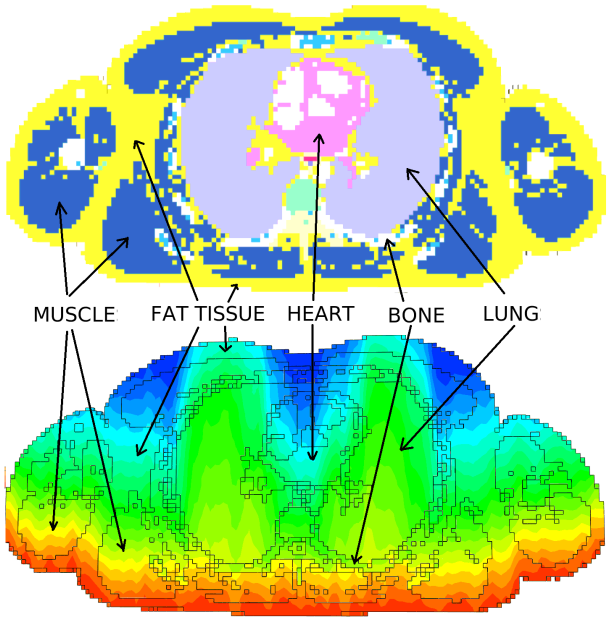

Figure 7: Cross sectional view on the transverse plane of the VIP-Man showing the anatomy (*top*) and flux tally (*bottom*) of a Posterior-Anterior directional photon gamma source, viewed in Abaqus/CAE

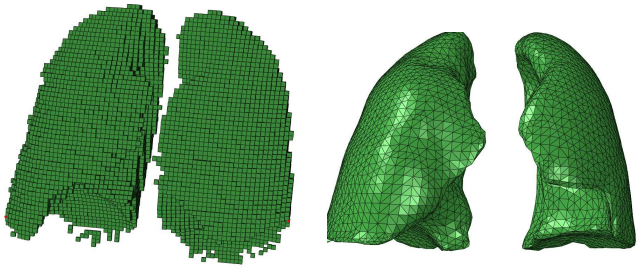

Figure 8: Lungs of the VIP-Man in Voxelized Abaqus *(left)* and Unstructured *(right)*

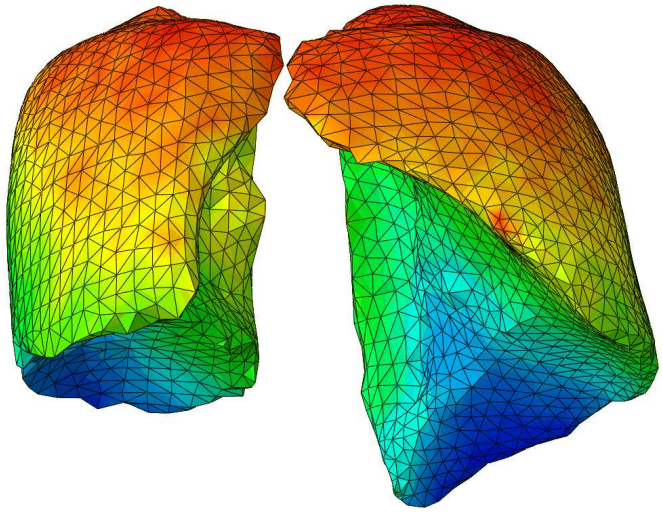

Figure 9: Gamma irradiation of the unstructured lungs

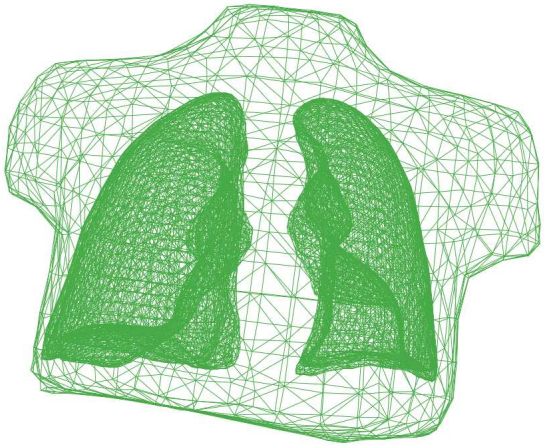

Figure 10: Unstructured mesh representation of the chest & lungs of the RPI-AM

ality with particle transport in MCNP. Once proven as a viable source, the voxelization requirement will no longer be needed from tomographic models, paving the way for a new era in particle transport with human phantoms.

V. Conclusion

The use of unstructured meshed human phantoms has great potential for the advancement of computational medical physics applications. Computational human phantoms are used for a variety of medical applications, such as tissue/organ deformation following surgery,[8] respiratory and biological modeling,[13] linear accelerator calibration, and dose assessment,[11,14,15,19] providing a gradually improving understanding of interactions within the human body. Patient-specific meshed models, generated from software such as 3D-Doctor,[3] could be used for Monte Carlo based treatment planning and post-treatment analysis as a more accurate alternative to the mathematical based ray-tracing technique currently used in many radiotherapy procedures.[16] Detailed whole body phantoms and improved computational analysis can develop better tissue interaction data, specific absorbed fractions, and weighting factors for particles in the body. Combination analysis from surgical procedures, respiratory modeling, and radiotherapy treatment with the same patient FEM could be a process used in the near future. Further testing of this capability is needed, but currently shows promising results of using the next generation of computational human phantoms for use in radiological dose assessment.

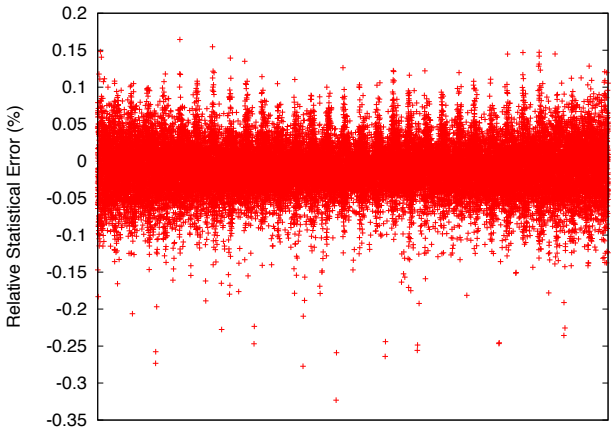

Figure 11: Mesh Tally Relative Statistical Error between the Abaqus mesh and CSG for 100 million histories

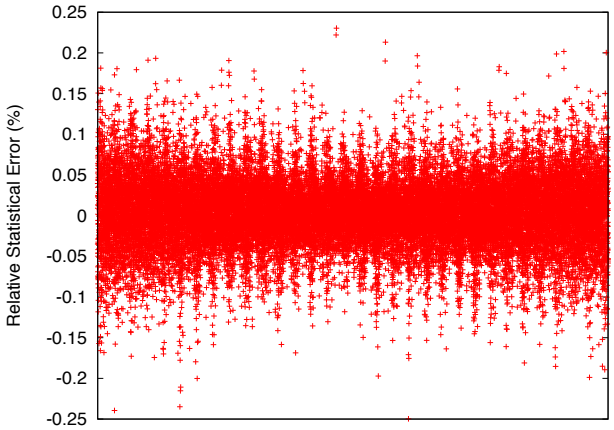

Figure 12: Mesh Tally Relative Statistical Error between the Abaqus mesh with and without the air voxels for 100 million histories

VI. Acknowledgements

- Dr. X. George Xu for the VIP-Man
- Dr. Paul Segars for the XCAT Phantoms
- Roger Martz for MCNP hybrid capatilities
- Chelsea D'Angelo for V & V and testing of the hybrid geometries

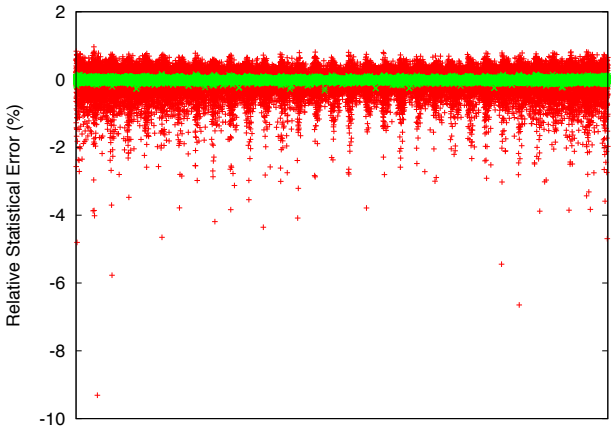

Figure 13: Abaqus and CSG mesh Tally Difference for 1 million (*red*) and 100 million histories (*green*)

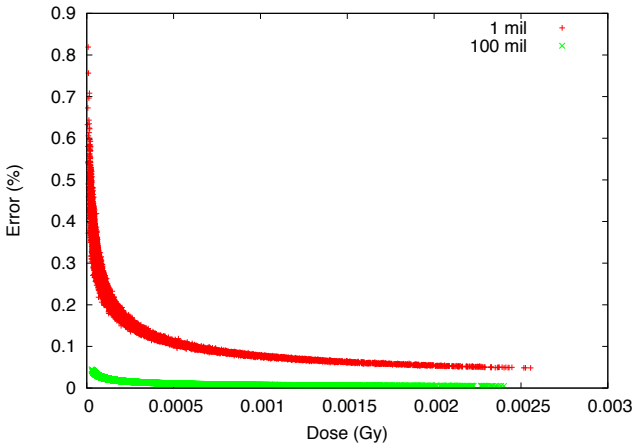

Figure 14: Dose Error Plot for 1 million (*red*) and 100 million histories (*green*)

References

[1] Unstructured mesh generation from the virtual family models for whole body biomedical simulations. *Procedia-Computer Science*, 1:837–844, 2010.

[2] X. George Xu Brian Wang. Issues related to the use of mcnp code for an extremely large voxel model vip-man. 98(E2):3247–3259.

[3] Able Software Corporation. 3d-doctor. `http://www.ablesw.com/3d-doctor/`, January 2012.

[4] J. T. Goorley, W.S. Kiger III, and R. G. Zamenhof. Reference dosimetry calculations for neutron capture therapy with comparison of analytical and voxel models. *Medical Physics*, 29:145–156, 2008.

[5] John T. Goorley. Mcnp medical physics geometry database, la-ur-05-6921 and la-ur-04-8518, 2005.

[6] T. Goorley, M. James, T. Booth, F. Brown, J. Bull, L.J. Cox, J. Durkee, J. Elson, M. Fensin, R.A. Forster, J. Hendricks, H.G. Hughes, R. Johns, B. Kiedrowski, R. Martz, S. Mashnik, G. McKinney, D. Pelowitz, R. Prael, J. Sweezy, L. Waters, T. Wilcox, and T. Zukaitis. *Initial MCNP6 Release Overview, submitted to Nuclear Technology, LA-UR-11-05198*. 2011.

[7] Choonsik Lee, Daniel Lodwick, Jonathan Williams, and Wesley Bolch. Hybrid computational phantoms of the 15-year male and female adolescent: Applications to ct organ dosimetry for patients of variable morphometry. *Medical Physics*, 35:2366 – 2382, 2008.

[8] Ashraf Mohamed and Christos Davatzikos. Finite element mesh generation and remeshing from segmented medical images.

[9] U.S. National Library of Medicine. The visible human project. `http://www.nlm.nih.gov/research/visible/visible_human.html`, Sept 2011.

[10] Committee II of the ICRP. *Report of the Task Group on Reference Man: ICRP Publication 23*. Pergamon Press, 1974.

[11] International Commission on Radiation Units and Measurements. *Phantoms and Computational Models in Therapy, Diagnosis, and Protection; ICRU Report 48*. 1992.

[12] International Commission on Radiation Units and Measurements. *Photon, electron, proton and neutron interaction data for body tissues; ICRU Report 46*. 1992.

[13] W.P. Segars. Modeling respiratory motion variations in the 4d ncat phantom. *IEEE*, 2007.

[14] W. S. Snyder, M. R. Ford, G. G. Warner, and Jr H. L. Fisher. Estimates for absorbed fractions for monoenergetic photon sources uniformly distributed in various organs of a heterogeneous phantom. *Journal of Nuclear Medicine*, 47, 1969.

[15] Bozkurt X. George Xu, T.C. Chao. VIP-Man: An Image-based Whole-body Adult Male Model Constructed from Color Photographs of the Visible Human Project for Multi-Particle Monte Carlo Calculations. *Health Physics*, 78:476–486, 2000.

[16] W Xiong1, D Huang, L Lee, J Feng, K Morris, E Calugaru, C Burman, J Li, and C-M Ma. Implementation of monte carlo simulations for the gamma knife system. *Journal of Physics: Conference Series*, 74, 2007.

[17] X. George Xu. Recent progress on computational phantoms and applications to imaging and therapy, 2010.

[18] X. George Xu and Keith F. Eckerman. *Handbook of Anatomical Models for Radiation Dosimetry, 1st edition*. Taylor & Francis, 2009.

[19] I.G. Zubal, C.R Harrell, E.O. Smith, Z. Rattner, G. Gindi, and P.B. Hoffer. Computerized three-dimensional segmented human anatomy. *Medical Physics*, 21:299–302, 1994.